Large-scale fabrication of decoupling coatings with promising robustness and superhydrophobicity for antifouling, drag reduction, and organic photodegradation

Lei XIN[1], **Hao LI**[1,*], **Jian GAO**[1], **Zhongwei WANG**[1], **KaiJie ZHOU**[1], **Sirong YU**[2]

[1] *School of Materials Science and Engineering, Shandong University of Science and Technology, Qingdao 266590, China*
[2] *School of Materials Science and Engineering, China University of Petroleum (East China), Qingdao 266580, China*

© The author(s) 2022.

Abstract: It is still a challenge to achieve large-area preparation of robust superhydrophobic surfaces with strong mechanical stability. Here, a simple and low-cost method to prepare robust decoupling superhydrophobic coatings on aluminum (Al) alloys substrate has been presented. The superhydrophobicity and robustness of decoupling coatings are realized by structuring surfaces at two different length scales, with nanostructures for superhydrophobicity and microstructures for robustness. This prepared decoupling coating shows promising superhydrophobicity, with water contact angle (CA) of ~158.4° and roll off angle (RA) of ~3°. It also exhibits high repellency for impacting water droplets. Notably, the decoupling coating processes outstanding adhesion strength on the substrate after tape-peeling and cross-cut tests, also with promising wear resistantance after sandpaper abrasion and wear test. The friction coefficient of this decoupling coating is only ~0.2. In addition, the robust decoupling superhydrophobic coating is applied to underwater buoyancy enhancement and fluid resistance reduction (drag reduction rate ~30.09%). This decoupling superhydrophobic coating also displays promising self-cleaning and antifouling properties. Moreover, benefitting from the photocatalytic property of TiO_2, this decoupling coating is also exploited for degrading organics to achieve seawater purification. This obtained decoupling superhydrophobic coating is expected to apply on other solids in marine fields, and the simple and eco-friendly method develops the potential practical application.

Keywords: Superhydrophobic; decoupling; wear resistance; drag reduction

1 Introduction

Inspired by natural superhydrophobic materials such as lotus leaves [1], researchers fabricated numerous superhydrophobic surfaces for self-cleaning [2], antifouling [3], drag reduction [4], etc. The chemical composition with low surface energy and micro/nano structures are two factors for superhydrophobicity [5]. Various approaches are applied to fabricate superhydrophobic surfaces such as spraying [6], electrodeposition [7], sol–gel method [8], etc. Nevertheless, some superhydrophobic coatings on the metal substrate are susceptible to damage because their

microstructures are subject to mechanical abrasion, also with impossibility for large-scale fabrication [7, 9]. Therefore, it is desired to improve the durability of superhydrophobic coatings and provide a simple method for large-scale fabrication.

To improve robustness of superhydrophobic coatings, methods such as nanosecond laser ablating or etching metal substrate were applied to increase the wear resistance of micro/nano structures [10, 11]. Moreover, Wang et al. [11] recently fabricated interconnected micro-structures as armors to protect hydrophobic nanostructures from mechanical damage, which inspired our study. Thus, there is an impetus

to improve the robustness of superhydrophobic coatings by fabricating micro-nano structures, in which the microstructure promises the robustness, and the nanostructure provides the hydrophobicity (namely "decoupling"). Although these methods prominently promoted wear resistance of superhydrophobic coatings, they are expensive and not enable for large-scale production. Several papers demonstrated that the robust superhydrophobic coatings were achieved by the one-step spraying method without introducing fluorine [12, 13]. For example, Li et al. [12] fabricated a robust superhydrophobic coating by one-step spraying a fluorine-free suspension composed of epoxy resin (EP), polydimethylsiloxane (PDMS), and modified silica (SiO_2) on various substrates. Nevertheless, for the one-step spraying method, the adhesive material also subjects to modify in the mixed suspension [13], which increases material usage and costs. Thus, there is an impetus to fabricate a robust decoupling superhydrophobic coating by spraying modified micro/nano particles on the adhesive layer without modification, which is more competitive in applications.

Possessing low density and high strength, aluminum (Al) and its alloys are widely used in marine fields, such as ships, submarines, underwater detectors, and other navigating bodies [14]. Nevertheless, it is subject to large seawater frictional resistance during navigation [15]. In addition, biofouling on Al (and its alloys) imposes negative impacts in marine environments, and thus limits their usages [3]. Superhydrophobic coatings show promising drag reduction, antifouling, self-cleaning, and other properties [16, 17], which is often desired to solve the above problems. Moreover, there are undegraded organics in seawater, which seriously affect the environment and aquatic organisms [18]. Recently, photocatalysis receives great attention due to its eco-friendly and sustainable route [19, 20]. Photodegradation of organics is the promising method for reducing water-soluble organic dyes in wastewater [21, 22]. Thus, it is anticipated that the fabrication of a robust decoupling superhydrophobic coating on Al alloy substrate for antifouling property, drag reduction, and photodegradation by spraying modified micro/nano TiO_2 particles on the adhesive layer.

In this study, we fabricated a robust decoupling superhydrophobic coating on Al alloy substrate. The unmodified micro SiO_2 particles were sprayed on the EP adhesive layer, which promised the robustness. Then, the modified nano TiO_2 particles were quickly sprayed on the surface, which provided the hydrophobicity. The adhesion strength of the prepared decoupling superhydrophobic coating was characterized via tape peeling and cross-cut tests. The wear resistance of this decoupling coating was verified by sandpaper abrasion and wear test. The hull loading experiment and the fluid drag reduction experiment were also conducted. Moreover, the obtained decoupling superhydrophobic coating was tested for self-cleaning, antifouling, and photocatalytic degradation properties.

2 Experimental

2.1 Chemicals and materials

The 5052 Al alloy samples (30 mm × 30 mm × 5 mm) were used as the substrate, which were first abraded by SiC papers of 400#, 1000#, 1500#, and 2500#, and then subsequently cleaned by absolute ethanol (C_2H_5OH) with ultrasonics for 10 min. EP and curing agent were supplied by Shanghai Nalle New Material Co., Ltd., China. Micro SiO_2 particles (10 μm, 99.0%) and nano TiO_2 particles (25 nm, 99.0%) were purchased from Aladdin Co., Ltd., China. Stearic acid ($CH_3(CH_2)_{16}COOH$), sodium chloride (NaCl), sodium hydroxide (NaOH), concentrated sulfuric acid (H_2SO_4), glycerol ($C_3H_8O_3$), and absolute ethanol (C_2H_5OH) were all analytical reagents (ARs) and purchased from Sinopharm Co., Ltd., China. All the reagents were used as received. Seawater was obtained from the Yellow Sea in Qingdao, China.

The unmodified micro SiO_2 particles suspension was obtained by dispersing 6.0 g of micro SiO_2 particles into 50 mL of ethanol with ultrasonics for 20 min. The nano TiO_2 particles were modified by stearic acid to improve their hydrophobicity. The suspension was obtained by adding 6 g of nano TiO_2 particles into 100 mL of 1 wt% stearic acid ethanol solution. Then, the mixed solution was dispersed ultrasonically for 20 min and magnetically stirred

for 2 h. In addition, the modified micro SiO_2 particles suspension was fabricated by adding 6 g of micro SiO_2 particles into 50 mL of 1 wt% stearic acid ethanol solution with ultrasonics for 20 min and magnetic stirring for 2 h. The modified SiO_2 and TiO_2 mixed suspension was prepared by dispersing 4 g of micro SiO_2 particles and 2 g of nano TiO_2 particles into 100 mL of 1 wt% stearic acid ethanol solution, and then treated it with the same method as above.

2.2 Preparation of decoupling superhydrophobic coating

The mixed solution of EP (4 g), curing agent (2 g), and absolute ethanol (20 mL) was dripped onto the pre-treated Al alloy surface as the adhesive layer. After the EP adhesive layer reaching the semi-cured state (60 °C, 20 min), the prepared micro/nano particles suspension was quickly sprayed onto the semi-cured adhesive layer.

For fabricating the decoupling superhydrophobic coating (Fig. 1(a)), the prepared unmodified micro SiO_2 particles were sprayed onto the semi-cured EP using 0.4 MPa compressed air, with the spraying distance of ~15 cm and the spraying time of ~10 s. Then, the prepared modified nano TiO_2 particles was quickly sprayed onto the SiO_2–EP coating. After dried in an oven at 60 °C for 2 h, the decoupling superhydrophobic coating was obtained on the Al alloy sample.

To compare and verify the robustness of the decoupling superhydrophobic coating, three other superhydrophobic coatings—micro coating, nano coating, and coupling coating were also prepared. For the micro coating, only modified micro SiO_2 particles were sprayed onto the semi-cured EP (Fig. 1(b)). For the nano coating, only modified nano TiO_2 particles were sprayed onto the semi-cured EP (Fig. 1(c)). For the coupling superhydrophobic coating, the modified micro SiO_2 and nano TiO_2 particle-mixed suspension was sprayed onto the semi-cured EP (Fig. 1(d)). Other conditions are the same as the fabrication of the decoupling superhydrophobic coating.

2.3 Characterizations and tests

The surface morphologies of the samples after Pt sputtering were investigated by the field emission scanning electron microscope (FE-SEM; FEI, Nova Nano 450, USA). The energy-dispersive X-ray spectroscopy (EDS; matched with the FE-SEM) was applied to analyze the element composition. The X-ray diffraction (XRD) patterns obtained by the X-ray diffractometer (D/Max2500PC, Japan) characterized the phase compositions of the samples. The Fourier transform infrared spectroscopy (FT-IR; NICOLET-SDXFl-IR, USA) was employed to analyze the chemical compositions of samples to determine the presence of low-energy materials. A multifunctional wear tester (CETR-UMT-3MO, USA) was used to test the robustness of samples. A three-dimensional topography (Zeta-20, USA) was used to obtain the three-dimensional morphology after wear test. The absorbance of solution was evaluated by the UV-visible spectrophotometer (EU-2600D, China). Water contact angles (CAs) on
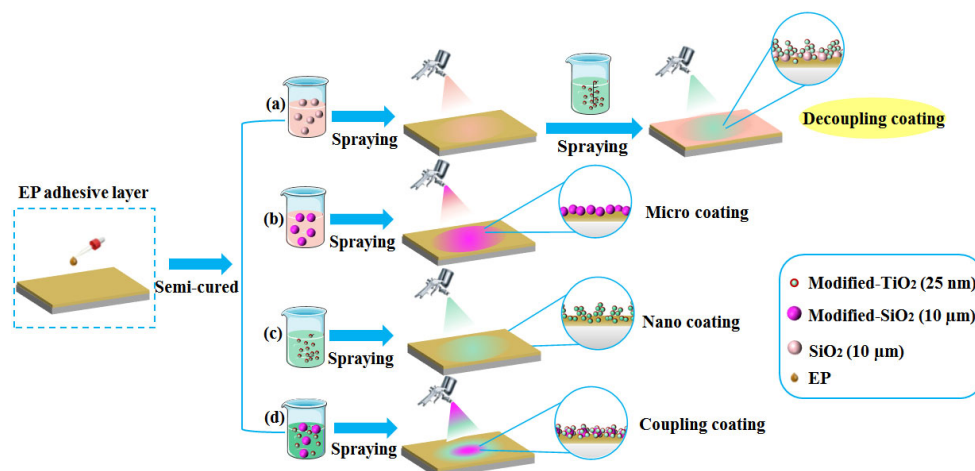

Fig. 1 Schematic illustration of the fabrication process for (a) decoupling coating, (b) micro coating, (c) nano coating, and (d) coupling coating.

the sample surface were measured by a CA meter (JC2000C1, China) in the air. To study the repellency for impact water droplets of the prepared samples, 12 μL (~3 mm in diameter) of water droplets were free-fall on coatings. A high-speed camera (Photron-FASTCAM UX 100, Japan) was used to record dynamics of droplets at 8,000 fps.

2.4 Robustness tests

To evaluate the adhesion strength between coatings and the substrate, tape peeling (3M 1500 tape) and cross-cut (ASTM D3359) tests were carried out. After peeling multiple times, CAs and roll off angles (RAs) of water droplets on coatings were measured. In the cross-cut test, a sharp knife was applied to cut crosshairs on coatings to ensure that coatings have been cut through. In addition, the samples were also immersed into 3.5 wt% NaCl solution and heating at 150 °C for different time. Different pH droplets and irradiation with UV-light (power 40 W) were applied to verify the chemical stability of coatings.

The mechanical durability of coatings was tested by the sandpaper abrasion. The sample was placed on the sandpaper (400#) and beneath a 200 g weight. The sample was pushed at different distances and CAs, and RAs after abrasion were measured to verify the wear resistance. To further evaluate the mechanical durability of coatings, a multifunctional wear tester for linear wear testing was employed, with a steel ball as the standard friction pair (GB308-84, diameter of 9.5 mm), a pressure of 5 N, the wear distance of 5 mm, and the wear time of 5 min.

2.5 Buoyancy increase and drag reduction tests

To study the carrying capacity of prepared coatings in water, different numbers of clips were placed on coatings to maintain a balance. The weight of a clip is ~0.45 g. The maximum load and the depth of water penetration of samples under different weights were recorded.

The drag reduction was carried out in a plastic tank (1.9 m × 0.45 m × 0.24 m). To investigate the drag reduction of the prepared coatings (Video S1 in the Electronic Supplementary Material (ESM)), each ship carried a 3 V battery as a power system and with the same weight. The time of the 1.7 m voyage was

recorded, and the average speed (v) of the model ship was calculated. This test was repeated 10 times.

2.6 Self-cleaning, photodegradation, and antifouling tests

Methylene blue (MB) powder was used for the self-cleaning test. MB powder was first distributed on the inclined decoupling coating (~RA), and then water droplets (~6 μL) were gently dropped on the contaminated surface. MB was also selected as an organic pollutant to evaluate the photodegradation property of the decoupling coating for organics. Coatings were immersed into a 0.0015 mol/L MB solution and irradiated under UV-light (power 40 W) for different time. To characterize the anti-biofouling property of the decoupling superhydrophobic coating, the sample was immersed into seawater for 7 days.

3 Results and discussion

3.1 Characterizations of decoupling superhydrophobic coating

It is well known that surface wettability is closely inseparable from low-surface-energy chemical compositions and micro/nano structures [23]. As shown in Fig. 2(a1), there are many micro-scale spherical protrusions covered with nano-scale particles on the decoupling coating, forming the micro-nano structure. The cross-sectional SEM image of the decoupling coating exhibits that the thickness of the EP adhesive layer is ~34 μm, and that of the sprayed micro-nano particles is ~18 μm (Fig. S1(a) in the ESM). It also indicates that the thickness of the EP adhesive layer and the micro-nano particle layer is uniform. As shown in Fig. 2(a2), the CA of water droplets on the decoupling coating is ~158.4°, with the RA of ~3° (Video S2(a) in the ESM), showing superhydrophobic. Bright "mirror" due to the total internal reflection at air–water interfaces was observed after the decoupling sample was immersed into water (Fig. 2(a4)), which is attributed to the air trapped among micro-nano structures [24]. In addition, the CA of glycerol droplets on this decoupling superhydrophobic coating is also more than 150° (Fig. 2(a3)), with the RA of ~5°, showing oleophobic. The chemical composition of the

decoupling superhydrophobic coating was verified by the EDS, XRD, and FT-IR. Elements of C (13.90 wt%), O (43.10 wt%), Si (21.25 wt%) and Ti (21.76 wt%) in the EDS spectrum (Fig. S2(a) in the ESM) and TiO_2 and SiO_2 peaks in the XRD patterns (Fig. S3 in the ESM) show that the micro-nano particles of the decoupling superhydrophobic coating are actually SiO_2 and TiO_2. Moreover, as shown in curve (I) of Fig. S4(a) in the ESM, the unmodified SiO_2 exhibits only two peaks of attributing bending and stretching vibrations of Si–O–Si bond at 1,092 and 802 cm^{-1}, respectively [12]. It indicates that the micro SiO_2 particles are unmodified. Curve (II) in Fig. S4(a) is TiO_2 nanoparticles modified by stearic acid. The characteristic peak of TiO_2 is at 520–880 cm^{-1}, indicating

the stretching vibration of the Ti–O bond [25]. The peak at 3,423 cm^{-1} corresponds to the hydroxyl (–OH) involved in the adsorption of H_2O [26]. There are sharp peaks near at 2,880 and 2,925 cm^{-1}, attributing to the C–H bonds in methyl (–CH_3) and methylene (–CH_2), respectively [12]. The asymmetric and symmetric stretching vibrations of carboxylate (COO–) are observed at 1,635 and 1,472 cm^{-1}, respectively [27]. It shows that the sprayed nano TiO_2 particles in the decoupling superhydrophobic coating were successfully modified by stearic acid. Thus, the low-surface-energy chemical compositions and micro-nano structures (unmodified micro SiO_2 and modified nano TiO_2) of the decouplig coating contribute to its promising superhydrophobic property.
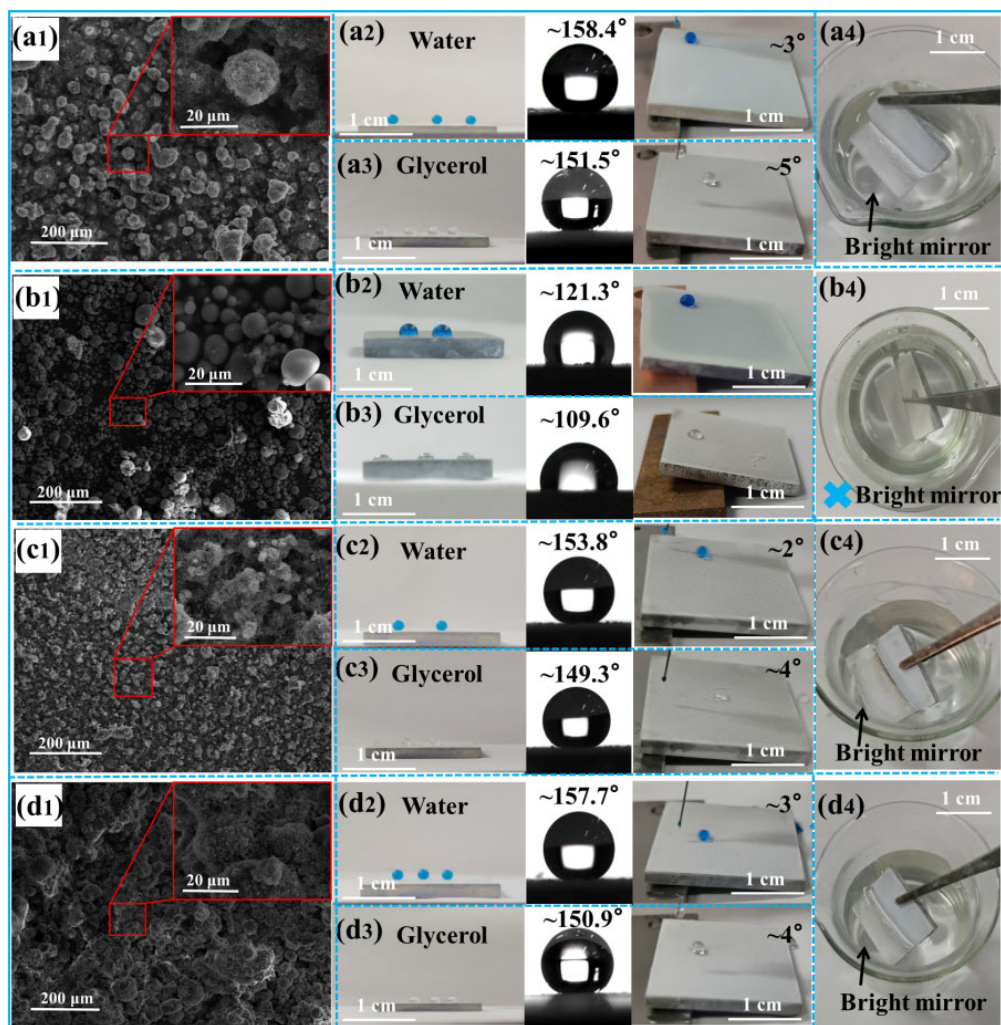

Fig. 2 SEM images of (a1) decoupling, (b1) micro, (c1) nano, and (d1) coupling coatings. Optical photographs, CAs, and RAs of water and glycerol droplets on (a2, a3) decoupling, (b2, b3) micro, (c2, c3) nano, and (d2, d3) coupling coatings. Optical photographs of (a4) decoupling, (b4) micro, (c4) nano, and (d4) coupling coatings immersion into water.

Compared the decoupling coating with other three coatings: micro, nano, and coupling coatings, the micro coating in Fig. 2(b1) shows that there are many microspheres, with water CA of ~121.3° (Fig. 2(b2)) and glycerol CA of ~109.6° (Fig. 2(b3), without bright "mirror" (Fig. 2(b4)). The chemical composition of micro coating in Figs. S2(b) and S4(b) in the ESM shows the modified SiO_2 on this coating. For the nano coating, there are many protrusions agglomerated by modified nano TiO_2 particles (Fig. 2(c1)), with water and glycerol CAs of ~153.8° (Fig. 2(c2)) and ~149.3° (Fig. 2(c3)), respectively. Water droplets quickly roll off on this coating with the RA of ~2° (Video S2(b) in the ESM). The chemical composition of nano coating in Figs. S2(c) and S4(c) in the ESM shows the modified TiO_2 on this coating. The coupling coating also shows micro-nano protrusions (Fig. 2(d1)), which is not obvious compared with the decouplig coating. These microspheres are almost covered by the nanoparticles, only with slight fluctuations under high-magnification images. This coating shows water and glycerol CAs of ~157.7° (Fig. 2(d2)) and ~150.9° (Fig. 2(d3)), respectively, and bright "mirror" (Fig. 2(d4)) also shows promising superhydrophobic property. Water droplets quickly roll off on this coating with the RA of ~3° (Video S2(c) in the ESM). The elements of the coupling coating shown in Figs. S2(d) and S4(d) in the ESM are the same as the decoupling coating, but with modified SiO_2.

Thus, the decoupling coating as well as nano coating and coupling coating exhibit promising superhydrophobicity, while the micro coating shows hydrophobicity. We only compared other properties of the decoupling superhydrophobic coating with nano superhydrophobic coating and coupling superhydrophobic coating in the following.

The water repellency of the decoupling superhydrophobic coating was further investigated. As shown in Fig. 3(a) and Video S3(a) in the ESM, when the droplet impacts on the decoupling coating surface, the droplet first deforms to multi-layer, and then spreads to the maximum diameter at 5.3 ms. In this process, the kinetic energy of the droplet is converted into the surface energy [28]. Once the droplet reaches the maximum contact diameter, as the surface energy converted into the kinetic energy, the droplet retracts [29]. Figure S5(a) in the ESM shows that the maximum contact diameter of droplet on the decoupling coating is 4.34 mm. Finally, the droplet bounces off the surface at 15.2 ms, and shows the maximum rebound height of 4.85 mm at 39.4 ms, with heights of 3.16 mm and 1.97 mm in the next two rebounds. During the first retraction, its receding velocity reaches the maximum of 0.44 m/s (Fig. S5(b) in the ESM). Compared with the nano coating (Fig. 3(b) and Video S3(b) in the ESM) and the coupling coating (Fig. 3(c) and Video S3(c) in the ESM), the maximum
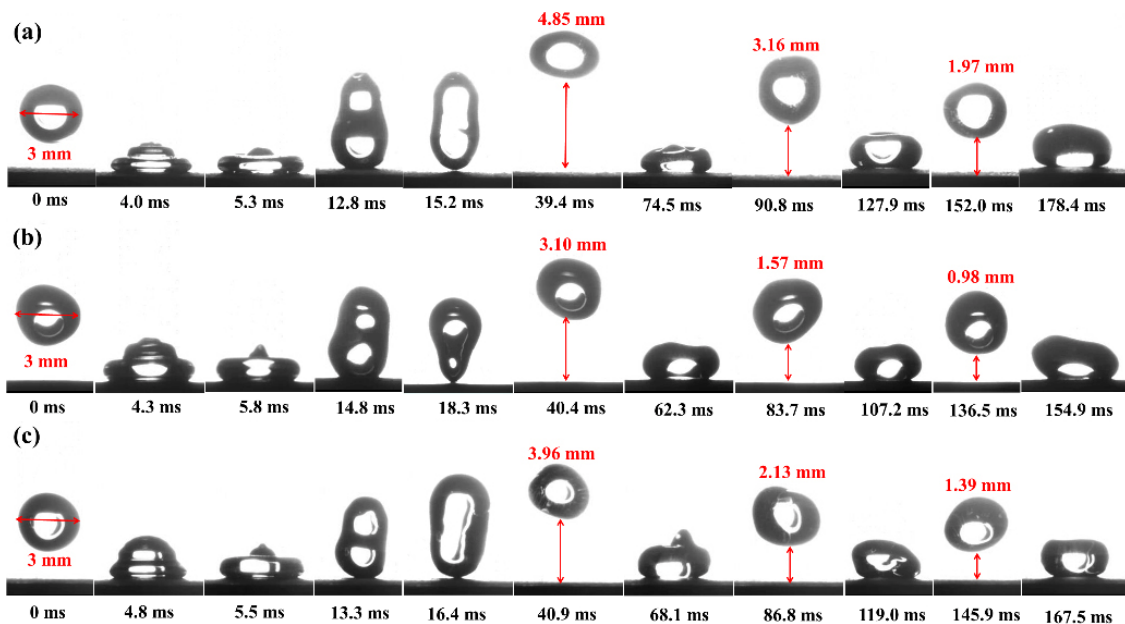

Fig. 3 Selected snapshots showing water droplet impacting on (a) decoupling, (b) nano, and (c) coupling coatings (v = 0.44 m/s).

retracted heights of these two coatings are 3.10 and 3.96 mm in the first retraction, respectively, which are prominently smaller than that of the decoupling coating. Moreover, Fig. S5(a) in the ESM displays the maximum contact diameter of the droplet on the decoupling coating is 4.34 mm, which is larger than that on the nano coating (3.53 mm) and the coupling coating (3.84 mm). It indicates that the energy consumption of the decoupling coating surface is the lowest [30]. This is because the micro-nano structure on the surface is prominent, with lots of air trapped in gaps, which protects water droplets penetrate into gaps, reducing the energy consumption [31]. Thus, the prepared decoupling superhydrophobic coating shows promising repellency for impacting water droplets.

3.2 Robustness of decoupling superhydrophobic coating

Robustness is important for superhydrophobic coatings in application. The damage of micro-nano structures or chemical compositions imposes negative impacts in its superhydrophobicity, and thus limits their usages [32]. The adhesion strength of superhydrophobic coatings

were usually characterized via tape peeling and cross-cut experiments [33]. Figure 4(a) shows the schematic illustration of the tape peeling test. The CAs and RAs of water droplets on these three superhydrophobic coatings (decoupling, nano, and coupling coatings) were measured after multiple cycles. Figure 4(b) shows that CAs and RAs of them are all remained above 150° and below 5°, respectively, after 19 tape peeling cycles. It indicates that these three coatings all possess robust adhesion strength. Moreover, the cross-cut test is applied to further evaluate the adhesion strength of these superhydrophobic coatings. Figure 4(c) shows the grid patterns of three coatings after cross-cut 100 times. There are no peeling marks on the grid edge of three coatings after the tape removed, without grid detached, and three coatings remains intact. Based on the standard ASTM D3359 [33], the adhesion of three coatings is all 5B. Compared with the other reports (Table 1), these three superhydrophobic coatings show prominent adhesion strength to substrate. This is because that EP as the adhesive layer with highly cross-linked three-dimensional network [12], and part of micro/nano particles were immersed into the semi-cured
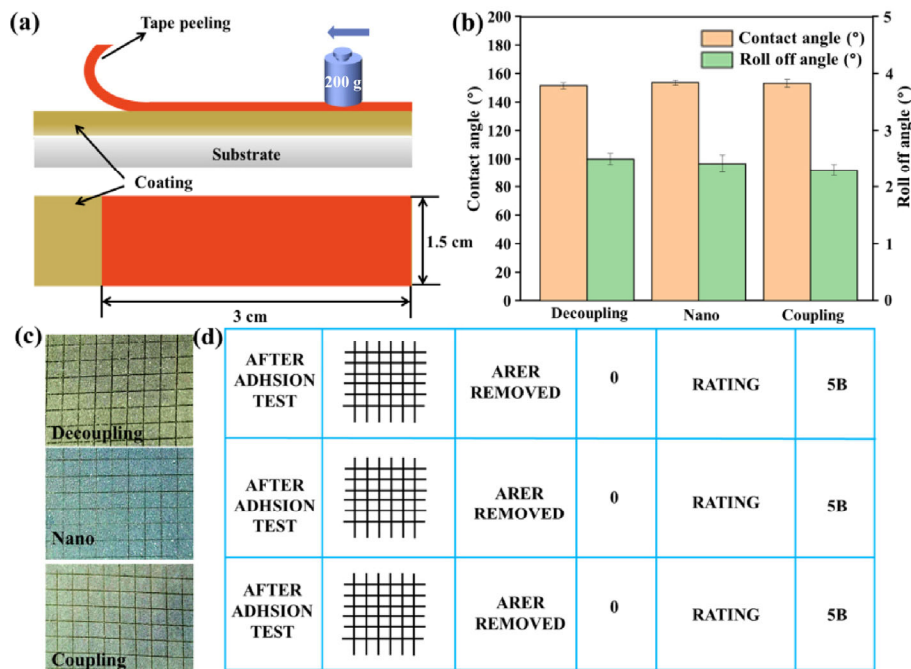

Fig. 4 (a) Schematic illustration of tape peeling test for coatings; (b) CAs and RAs of water on the decoupling, nano, and coupling coatings after 19 tape peeling cycles; and cross-cut test performed following ASTM standard D3359 for three coatings: (c) optical photographs of three coatings after cross-cut test and (d) three coatings showed 0 damage with ranking 5B.

Table 1 Comparison of robustness exhibited by our prepared superhydrophobic coatings with those of the other reports when the samples subjected to cross-cut and wear tests.

Coating/surface	Fabrication method	Cross-cut test	Wear test	Ref.
		Rating	Friction coefficient	
AP, HDTMS, SiO_2	Spraying	—	—	[35]
Polyvinylidene fluoride (PVDF), EP	Paint	4B	—	[36]
EP, Al_2O_3, KH560	Inverse infusion	4B	—	[9]
EP, SiO_2, KH570	Paint	4B	—	[37]
CP, MgO, AOP	Self-polymerization	4B	—	[38]
TiO_2/polysiloxane resin	Mixed paint	—	—	[39]
Ti/Cr	Plasma reverse sputtering process	—	0.528	[10]
ZIF-8, HDTMS, SiO_2	Etching	—	0.288	[40]
316L stainless steel	Laser melting	—	0.2228	[41]
Nano coating	Spraying	5B	0.6	This work
Coupling coating	Spraying	5B	0.3	This work
Decoupling coating	Spraying	5B	0.2	This work

EP adhesive layer, with the upper part exposed to air for superhydrophobic. In addition, as reported in Ref. [34], the chemical stabilities of these three coatings were studied by different pH droplets, UV irradiation for 24 h, immersion into 3.5 wt% NaCl solution for 9 d, and heating at 150 °C for 9 h. As shown in Figs. S6 and S7 in the ESM, the CAs and RAs of them are all ~150° and < 10°, respectively, showing stable chemical stability.

The wear resistance of these three superhydrophobic coatings was verified by sandpaper abrasion (Fig. 5(a)) and wear test (Fig. 7(a)). The CAs and RAs are measured as a function of the abrasion distance in Fig. 5(b). It shows that the decoupling coating maintains superhydrophobicity, with CA > 150° and RA < 5°, even after abrasion of 21 cm. The coupling coating loses its superhydrophobicity, with CA < 150° and RA > 5°, after abrasion of 19 cm. Nevertheless, the CA of the nano coating reduces to < 150° after abrasion of 13 cm, with RA > 5°. Optical pictures (Fig. S8 in the ESM) of three coatings after abrasion are also provided. There is damage on the surface of the nano coating (Fig. S8(b) in the ESM) and the coupling coating (Fig. S8(c) in the ESM) after abrasion of 5 cm, prominent after abrasion of 9 cm, while the decoupling coating retains intact (Fig. S8(a) in the ESM). It indicates that the decoupling coating displays better wear resistance of sandpaper abrasion than the

coupling coating and the nano coating. Figure 5(c) shows the surface morphologies of three coatings after abrasion of 9 cm. There are still many rough structures on the decoupling surface (Fig. 5(c1)). Although many nanostructures on the top of the surface are rubbed off, microstructures are still intact. Prominently, these microstructures effectively protect the lower body, and the entire surface shows a typical micro-nano structure. It is important for the superhydrophobicity of the coating. Nevertheless, the surface of the coupling coating is relatively flat (Fig. 5(c3)), with obvious scratches, and the original micro-nano structure is destroyed. Nanoclusters on the nano surface are worn prominently (Fig. 5(c2)), also with the obvious scratch. Thus, the decoupling superhydrophobic coating shows outstanding robustness for sandpaper abrasion compared with the nano and coupling superhydrophobic coatings.

Figure 6(a) shows the wear mechanism of three coatings. The micro SiO_2 particles immersed into the EP adhesive layer of the decoupling coating effectively protect the lower body (Fig. 6(a)I), which results in that only nanoparticles on top of the surface are damaged during abrasion. These microstructures enhances the wear resistance, and the entire surface maintains a typical micro-nano structure after abrasion. There are many nano TiO_2 particles agglomerated on the surface of the nano coating (Fig. 6(a)II). However,
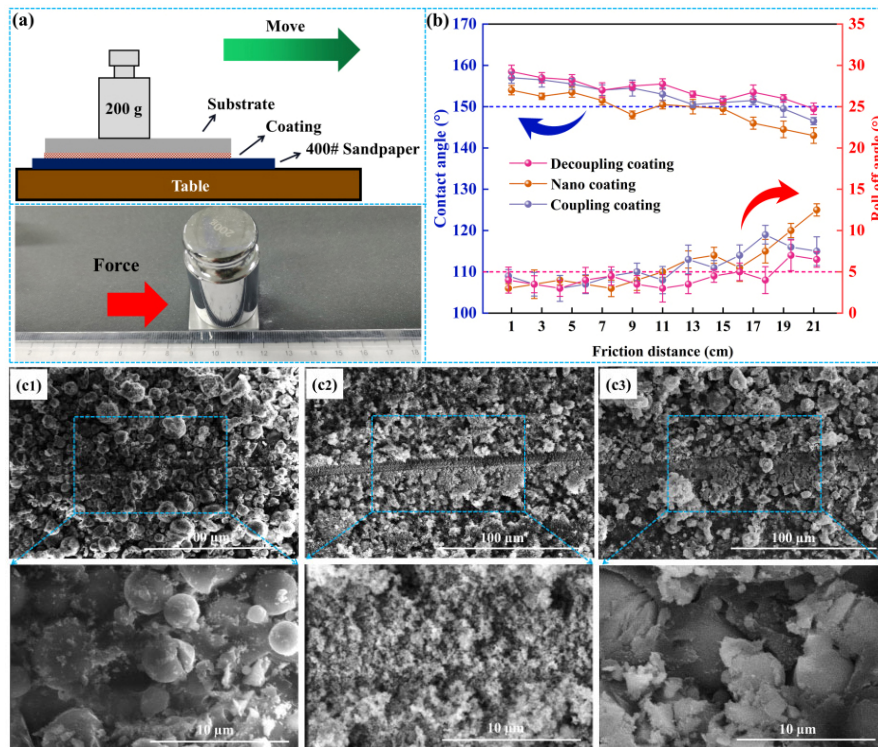
Fig. 5   (a) Schematic diagram of sandpaper abrasion test; (b) CAs and RAs of water droplets after abrasion for different distances; and SEM images of (c1) decoupling, (c2) nano, and (c3) coupling coatings after abrasion for 9 cm.
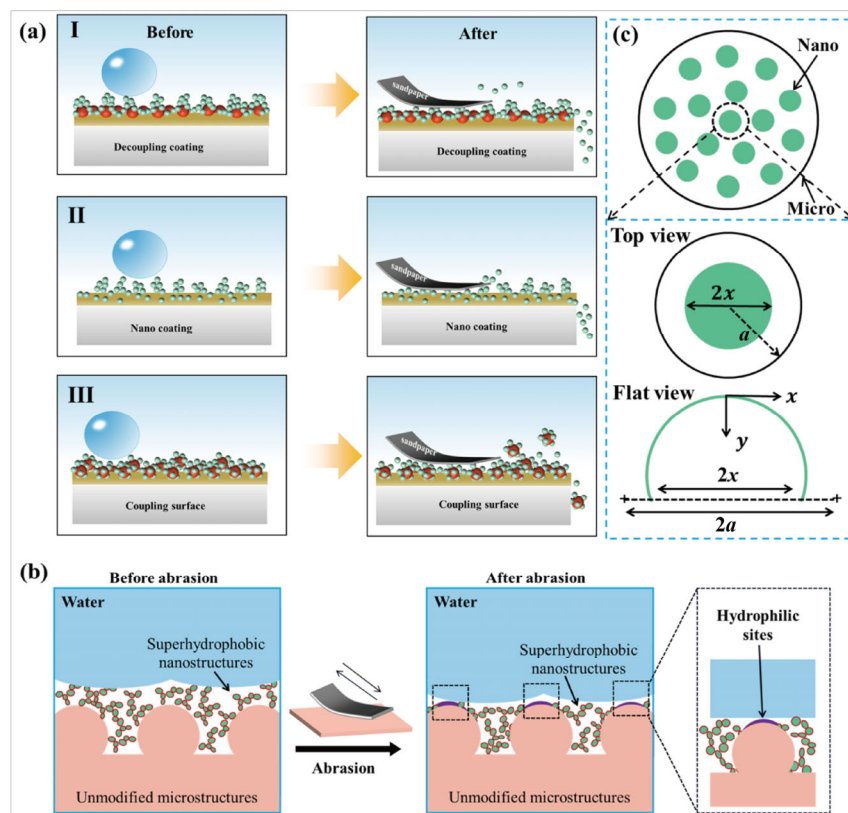

Fig. 6   (a) Schematic mechanism of three coatings before and after abrasion; (b) schematic mechanism of wear resistance on the decoupling superhydrophobic coating before and after abrasion; and (c) cross-section schematics of the decoupling superhydrophobic coating.

some of nanoparticles are damaged after abrasion, reducing the hydrophobicity. Micro SiO_2 particles covered by TiO_2 nanoparticles in the coupling coating are also damaged during abrasion (Fig. 6(a)III). As shown in Fig. 6(b), the mechanism of wear resistance on the decoupling coating is further explored. The surface of the unmodified micro SiO_2 structure exhibits superhydrophobic property after integrating the modified nano TiO_2 particles. It is worth noting that the wear test removes the modified nano TiO_2 particles from the top of the micro SiO_2 structure, which changes the local wettability of the surface from hydrophobic to hydrophilic [42]. The fractal nano structures between the micro structure frameworks remain intact. Wang et al. [11] pointed that the micro-scale gas–liquid–solid composite interface is prominently stable because the three-phase contact line is supported by local hydrophilic sites. Moreover, hydrophobic nano structures prevent the liquid–gas interface from sagging due to Laplace pressure [43], and the entire system remains in a constrained equilibrium Cassie state [44]. Figure 6(c) displays a schematic cross-section of the decoupling coating before and after sandpaper abrasion. As mentioned earlier [28], water droplets on the decoupling superhydrophobic coating show the Cassie state, and thus it is expressed as Eq. (1):

$$\cos\theta_{\text{before}}^{*} = f_{\text{before}}^{\text{micro}}(\cos\theta_{\text{r}}^{\text{micro}}+1) - f_{\text{before}}^{\text{nano}}(\cos\theta_{\text{r}}^{\text{nano}}+1) - 1 \tag{1}$$

where $\theta_{\text{before}}^{*}$ is the apparent CA, $f_{\text{before}}^{\text{micro}}$ and $\cos\theta_{\text{r}}^{\text{micro}}$ are defined as the liquid–solid contact fraction and Young's CA of microstructures, respectively. Moreover, $f_{\text{before}}^{\text{nano}}$ and $\cos\theta_{\text{r}}^{\text{nano}}$ are the liquid–solid contact fraction and Young's CA of nanostructures, respectively. These nanostructures on the microparticles are subject to wear when rubbing. Thus, the liquid–solid contact fraction before and after abrasion could be assumed unchanged. The nano structure is simply represented as a hemispherical model:

$$y = \sqrt{a^2 - x^2} \tag{2}$$

where x is the radial coordinate (the radius of the abrased surface on the nano structure, $0 < x \leqslant a$), y is the vertical coordinate measured downward form the apex (the abrasion height, $0 < y < \frac{a}{2}$), and a is the

radius for the selected nano structure. Before abrasion, the top of the nano structure is hemisphere, thus the liquid–solid contact fraction $f_{\text{before}}^{\text{nano}}$ is

$$f_{\text{before}}^{\text{nano}} = \frac{2\pi a\sqrt{a^2 - x^2}}{\pi a^2} \tag{3}$$

After abrasion, the Cassie state of the decoupling coating surface is [11, 28]:

$$\cos\theta_{\text{after}}^{*} = f_{\text{after}}^{\text{micro}}\left(\cos\theta_{\text{r}}^{\text{micro}}+1\right) + f_{\text{after}}^{\text{nano}}\left(\cos\theta_{\text{r}}^{\text{nano}}+1\right)-1 \tag{4}$$

The top of the nano structure is flat after abrasion, and thus $f_{\text{after}}^{\text{nano}}$ is

$$f_{\text{after}}^{\text{nano}} = \frac{\pi x^2}{\pi a^2} \tag{5}$$

Based on the above equations, it shows

$$\begin{aligned}
\cos\theta_{\text{after}}^{*} - \cos\theta_{\text{before}}^{*} &= f_{\text{after}}^{\text{nano}}\left(\cos\theta_{r}^{\text{nano}}+1\right)+ \\
&\quad f_{\text{before}}^{\text{nano}}\left(\cos\theta_{r}^{\text{nano}}+1\right) \\
&= \frac{\pi x^2}{\pi a^2}\left(\cos\theta_{r}^{\text{nano}}+1\right)+ \\
&\quad \frac{2\pi a\sqrt{a^2 - x^2}}{\pi a^2}\left(\cos\theta_{r}^{\text{nano}}+1\right) \\
&> 0
\end{aligned}$$

Thus,

$$\cos\theta_{\text{after}}^{*} > \cos\theta_{\text{before}}^{*} \quad (\text{i.e., } \theta_{\text{after}}^{*} < \theta_{\text{before}}^{*}) \tag{6}$$

The apparent θ^* of water droplets on the decoupling coating slightly decreased after abrasion (from 158.4° to 148.5°). Although it is desired to improve the wear resistance of this decoupling coating compared with that of *Wang* et al. [11], this method is prominently convenient and fast, and is suitable for real-world large-scale production.

The wear resistance of the prepared decoupling coating was verified by wear test (Fig. 7(a)). Figure 7(b) shows the friction coefficients of the bare Al alloy, EP coating, nano coating, coupling coating, and decoupling coating. The friction coefficient of EP coating (~0.6) is significantly lower than that of the bare Al alloy (~1.0), indicating the enhancement of the wear resistance. The friction coefficient of the stabilized EP coating (~0.4) is close to that of the nano coating. This is because these self-assembled clusters by nano particles are easily
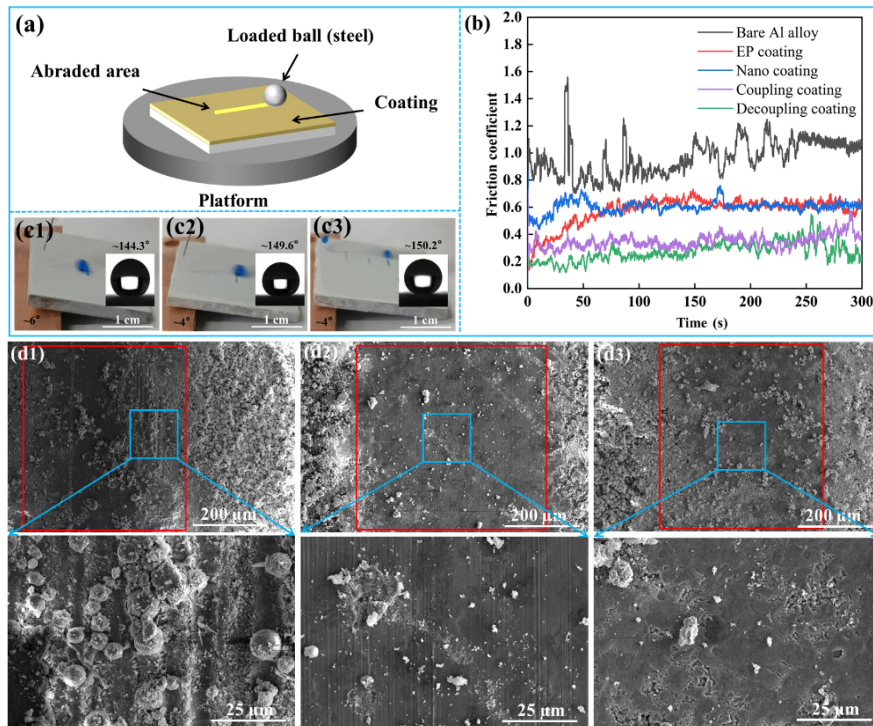
Fig. 7 (a) Schematic illustration of wear test for coating; (b) friction coefficients of bare Al alloy, EP, nano, coupling, and decoupling coatings; CAs and RAs of water on the (c1) nano, (c2) coupling, and (c3) decoupling coatings after wear test; and SEM images of (d1) decoupling, (d2) nano, and (d3) coupling coatings after wear test.

rubbed off, also indicating that the wear resistance of the nano coating is weak. This is because these self-assembled clusters by nano particles are rubbed off after 50 s, also indicating that the wear resistance of the nano coating is weak. The friction coefficients of the coupling coating (~0.3) and the decoupling coating (~0.2) with micro-nano composite structure are prominently lower than those of the EP coating and the nano coating within 300 s. There is few reports measuring the friction coefficient of superhydrophobic coatings by wear test. As shown in Table 1, researches on measuring the friction coefficient are the fabrication of superhydrophobic coatings by high-cost methods such as laser and templating [10, 38, 39], in which the friction coefficients are larger than that of this decoupling coating. It indicates that the decoupling coating improved the wear resistance via convenient and efficient fabrication method. Moreover, optical pictures of coatings after the wear test is shown in Fig. S9 in the ESM. The wear traces of the decoupling coating are the weakest (Fig. S9(a) in the ESM), followed by the coupling coating (Fig. S9(c) in the ESM), and the wear traces of the nano coating are noticeable

serious (Fig. S9(b) in the ESM). Moreover, the SEM images of coatings after the wear test are shown in Figs. 7(d1)–7(d3). These low-magnification SEM images show abraded areas of micro-nano structures on all three coatings (within red boxes) after 300 s of wear test. However, the scratched area of the decoupling coating is observed at the high-magnification SEM image (Fig. 7(d1)), and these microsphere particles are not completely damaged. In contrast, the scratched region of the nano coating shows flat, without prominent micro/nano structures (Fig. 7(d2)). The micro-nano structure of the coupling coating is also damaged, and there are some wear pits on the coating surface (Fig. 7(d3)). Figure S10 in the ESM shows the three-dimensional topographies of three coatings after the wear test. There are bright white depressions in the middle of surfaces, which are scratches after the wear test. It is worth noting that the depression of the nano coating reaches 1,003.24 μm, followed by the coupling coating of 897.80 μm, and the concave depth of the decoupling coating is the smallest (501.54 μm). It also indicates that the excellent wear resistance of the decoupling coating. It is because of

the synergistic effect of the EP adhesive layer and unmodified micro SiO_2 particles immersion into the adhesive layer with modified nano TiO_2 particles for superhydrophobicity. Thus, it confirms that the decoupling superhydrophobic coating shows outstanding wear resistance by comparing with the nano superhydrophobic coating and the coupling superhydrophobic coating.

3.3 Buoyancy increase and drag reduction of decoupling superhydrophobic coating

The unique wettability of superhydrophobic surfaces could effectively enhance the loading capacity of objects floating on the water [15]. To investigate the ability of the decoupling superhydrophobic coating in increasing the loading capacity, glass slices were used as the samples, and paper clips were as the load. As displayed in Fig. 8(a), the coated and uncoated samples are placed horizontally on the water surface.
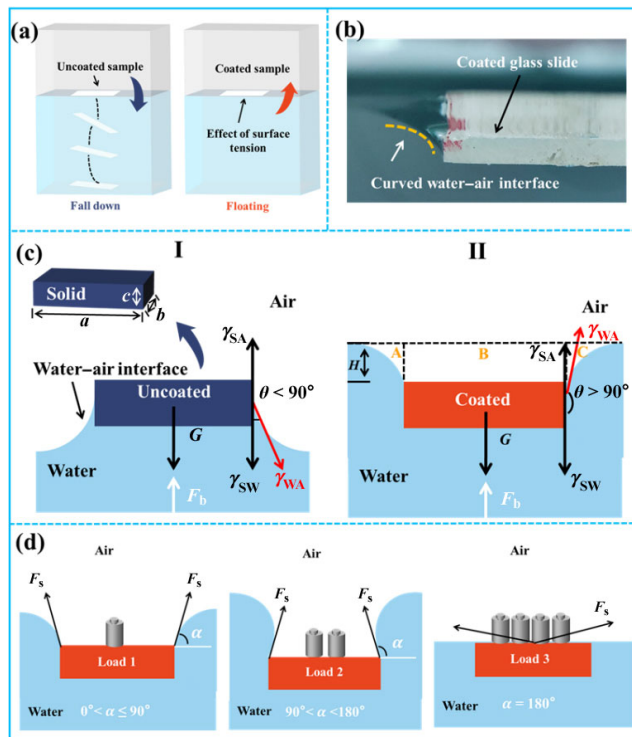

Fig. 8 Floating mechanism of a superhydrophobic body on the water surface based on surface tension. (a) Schematic diagram of the buoyancy test for uncoated and coated samples. (b) Optical image of top surface-coated glass slides floating on the water surface: cross-section. (c) Relationship between surface tension and wettability: hydrophilic and hydrophobic. F_b denotes buoyant force. (d) Schematic diagram of hydrophobic objects pressing into the water surface.

The uncoated (hydrophilic) sample directly falls down into water, while the coated (superhydrophobic) sample still floats on water due to the surface tension of the water. Figure 8(c) shows the mechanism of difference in buoyancy between the uncoated and coated samples, which is related to the water–gas–solid contact interface [45–57]. When the uncoated sample is put into water, the water surface is concave, and the interfacial tension direction (γ_{WA}) is downward due to the uncoated sample is hydrophilic ($\theta < 90°$) (Fig. 8(c)I). Conversely, the coated sample surface shows a large water CA ($\theta > 150°$), which results in the water surface convex and the upward of γ_{WA} (Fig. 8(c)II). When the superhydrophobic sample floats on the water, a liquid–air interface forms at the sample wedge. As the load weight increases, the arc of interface is more curved (Fig. 8(b)). The gravitational force of the discharged water in the water–air–solid triple contact regions and the surface tension even in the vertical direction are main reasons for the increased buoyancy of the superhydrophobic coating [45–47]. The vertical force (supporting force, F_L) of the superhydrophobic sample is described as [45–47]:

$$F_L = \rho abcg + \rho abH + 4\gamma_{WA}(a+b) \qquad (7)$$

where a, b, and c is the geometric parameters of the sample, H is the distance between water surface and sample surface, and γ_{WA} is the water surface tension. Thus, when the sample size is constant, F_L in the vertical direction is related to the load weight. As the load weight increases, the support force induced by the surface tension decreases. As shown in Fig. 8(d), the support force induced by surface tension no longer exists, and the superhydrophobic sample sinks into water when the inclination angle (α) eventually becomes parallel to the water surface.

Moreover, the load-carrying capacity of three superhydrophobic coatings were investigated. As shown in the Fig. 9 and Fig. S11 in the ESM, when the load of the decoupling coating increases to 2.70 g, the sinking depth reaches 4.43 mm, with the sample floating on the water surface. This is because the air trapped among gaps of micro-nano structures, which prevents water from penetrating into the void [46]. The sinking depth of the nano coating is 2.74 mm when the load is 1.35 g. Moreover, the sinking depth
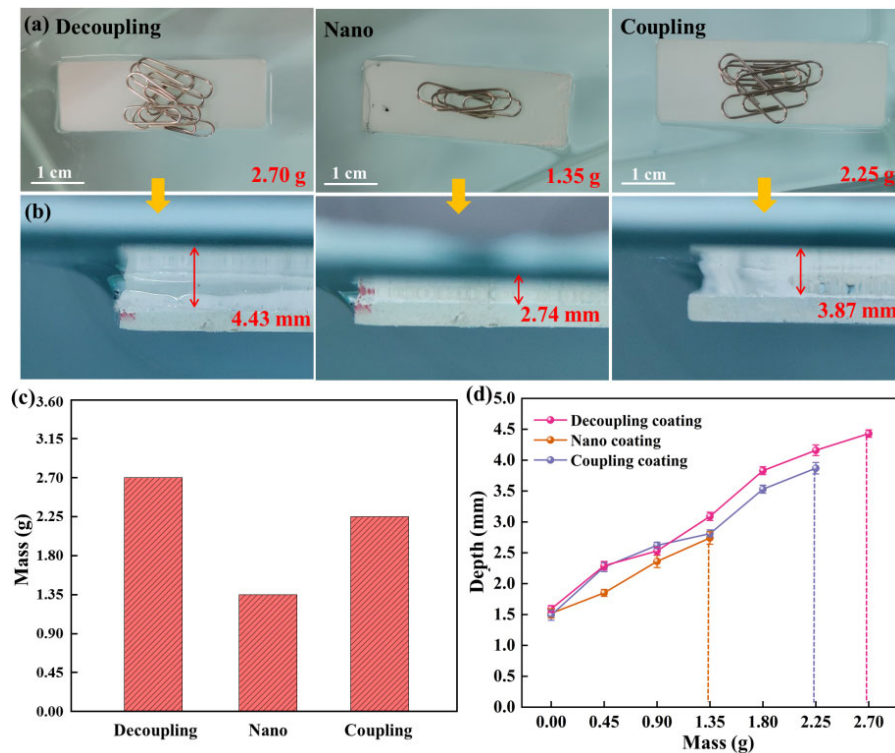
Fig. 9 (a) Optical images of maximum load carried by the decoupling, nano, and coupling coatings; (b) optical images of maximum depth of three coatings sinking into water; (c) carrying capacity of three coatings; and (d) depths of samples sinking into water as a function of load.

of the coupling coating is 3.87 mm as the load is 2.25 g. Nevertheless, the nano and the coupling samples would sink if the load continues to increase. Notably, the buoyancy increase of the decoupling coating is promising.

To demonstrate the drag reduction of the prepared decoupling coating in water, we conducted sailing experiments of model ships (Figs. 10(a) and 10(b) and Video S4 in the ESM), in which the bottom of model ship was with different coatings (Fig. 10(c)). The main reason for the drag reduction on the superhydrophbic coating is summarized as follows [49]: (1) When the superhydrophobic surface is in contact with water, the micro-nano structures on its surface forms an air film. The original solid–liquid interface converts into a gas–liquid interface and a solid–gas interface, thereby reducing friction caused by the liquid–solid contact. (2) The air trapped among gaps of micro-nano structures forms the gas–liquid interface with the external water flow, which causes interface boundary slip and reduces the friction between water and ship surface (Fig. 10(d)).

As shown in Figs. 11(a) and 11(b), compared with

the drag reduction rates of ships uncoated (namely 0%, Video S4(a) in the ESM), coated with the nano coating (~20%, Video S4(c) in the ESM) and the coupling coating (29.26%, Video S4(d) in the ESM), the drag reduction rate of the ship coated with the decoupling coating reaches up to 30.09% (Video S4(b) in the ESM), showing promising drag reduction, which is consistent with the aforementioned load-bearing experiment. Here, the equation for calculating drag reduction rate is

$$D = \frac{V_{\text{Coated}} - V_{\text{Uncoated}}}{V_{\text{Uncoated}}} \qquad (8)$$

Here, D is drag reduction rate, V_{Coated} is velocity of coated ship, and V_{Uncoated} is velocity of uncoated ship.

Figure 11(c) displays other researches on the drag reduction rates of superhydrophobic coatings in recent years. It demonstrates that drag reduction rates of most superhydrophobic coatings present below 25% [4, 13, 14, 50–55], while the drag reduction rate of this prepared decoupling coating reaches 30.09%. Thus, the prepared decoupling coating shows an outstanding improvement in drag reduction.
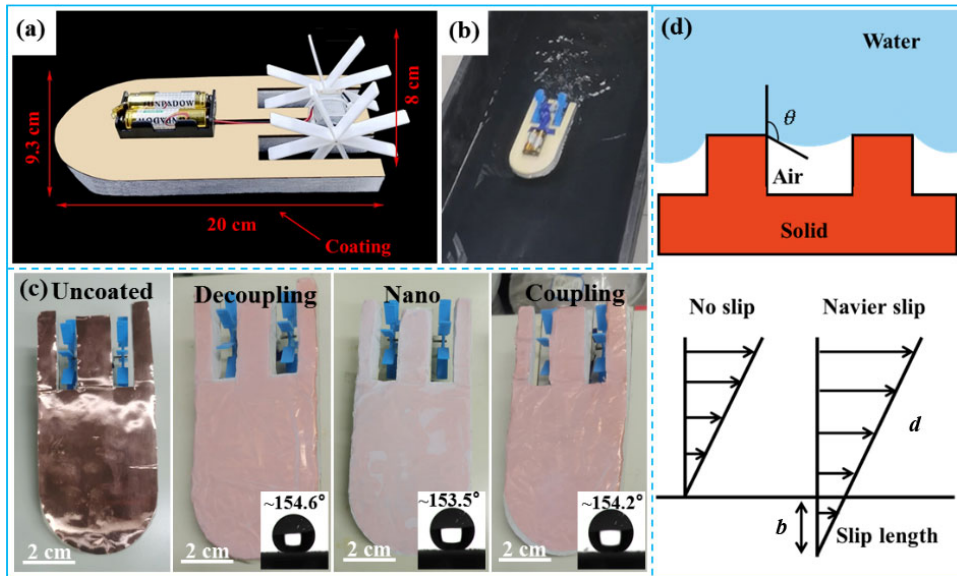
Fig. 10 (a) Boat model and (b) model ship sailing in water, (c) model boats with and without coating, and (d) drag reduction mechanism of coating underwater at air–water interface. θ is the solid–gas contact angle, b is slip length, and d is no slip length.
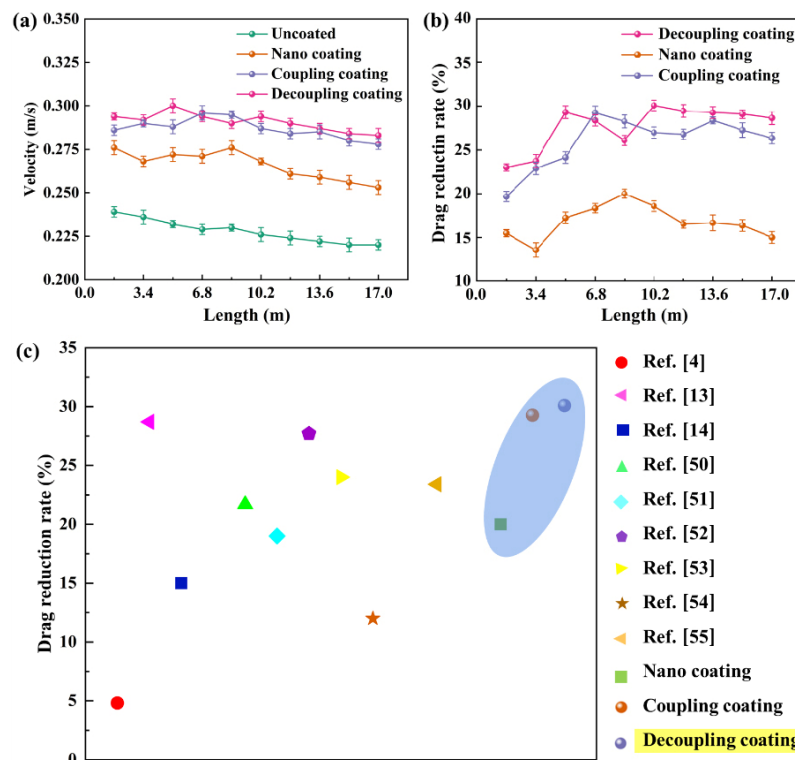

Fig. 11 Sailing tests of ships with and without coatings: (a) velocity; (b) drag reduction rate. (c) Comparison of drag reduction rate of superhydrophobic surfaces in recent years [4, 13, 14, 50–55].

3.4 Self-cleaning property of decoupling superhydrophobic coating

The self-cleaning property as one of the most desirable performances of superhydrophobic coating shows

effectively paved ways to clean the surface various contamination [7, 56–58]. Here, to investigate the self-cleaning property of the prepared superhydrophobic coating, MB powder was used as the simulated

contaminant. As displayed in Fig. 12(a), water droplets were gradually dripped onto the slightly tilted decoupling superhydrophobic coating, where some MB powder was sparsely deposited. The powder was immediately carried away by rolling water droplets, and no traces of water were left behind, contributing to a cleaned surface. These water droplets retained spherical shape during rolling. Thus, the decoupling superhydrophobic coating exhibits promising self-cleaning ability. In addition, nano coating and coupling coating also show outstanding self-cleaning property (Figs. 12(b) and 12(c), respectively). The self-cleaning mechanisms of three superhydrophobic coatings are shown in Fig. 12(e). Yu et al. [59] explained the self-cleaning property of the superhydrophobic surface was related to the surface force. Inspired by this, as shown in Fig. 12(d), the interface force (F_γ) on a superhydrophobic surface is inclined upward. The vertical component of F_γ would partially or fully counteract the adhesion force and gravity of the particle, while the horizontal component of F_γ drives particles to move along with the water droplet. Both horizontal and vertical components of F_γ contribute to self-cleaning. It is clear that when $\theta > 90°$, the larger the CA, the greater the vertical component force of F_γ. Thus, these pollutant particles are quickly

driven off three superhydrophobic coatings by water droplets, all showing promising self-cleaning property.

In addition, there are often organics dissolved in seawater, and these water-soluble dyes often disrupt the balance of aquatic ecosystems [60]. On account of the inherent photosensitivity of some hazardous organics, the photocatalytic degradation of organics is ideal for the efficient treatment of polluted seawater. TiO$_2$ is a desirable photocatalyst, which is widely applied in liquid purification due to its excellent photocatalytic performance and chemical stability [21, 22]. Here, MB powder was selected as the organic contamination to investigate the photocatalytic degradation of the decoupling coating. By immersing the decoupling superhydrophobic sample in MB solution, the absorption spectrum in Fig. 13(a) demonstrates that the absorbance at 664 nm decreases with the increase of the irradiation time. It is shown prominently in Fig. 13(b), and it can be observed that the colors of MB solutions gradually become lighter in turn. Figure 13(c) displays the variation of CAs of the decoupling coatings with the immersion time in MB solution. It is still above 150° after immersion for 24 h. The photocatalytic degradation of the decoupling coating is explained as follows (Fig. 13(d)) [61]: The electron–hole pairs generates and migrates to the
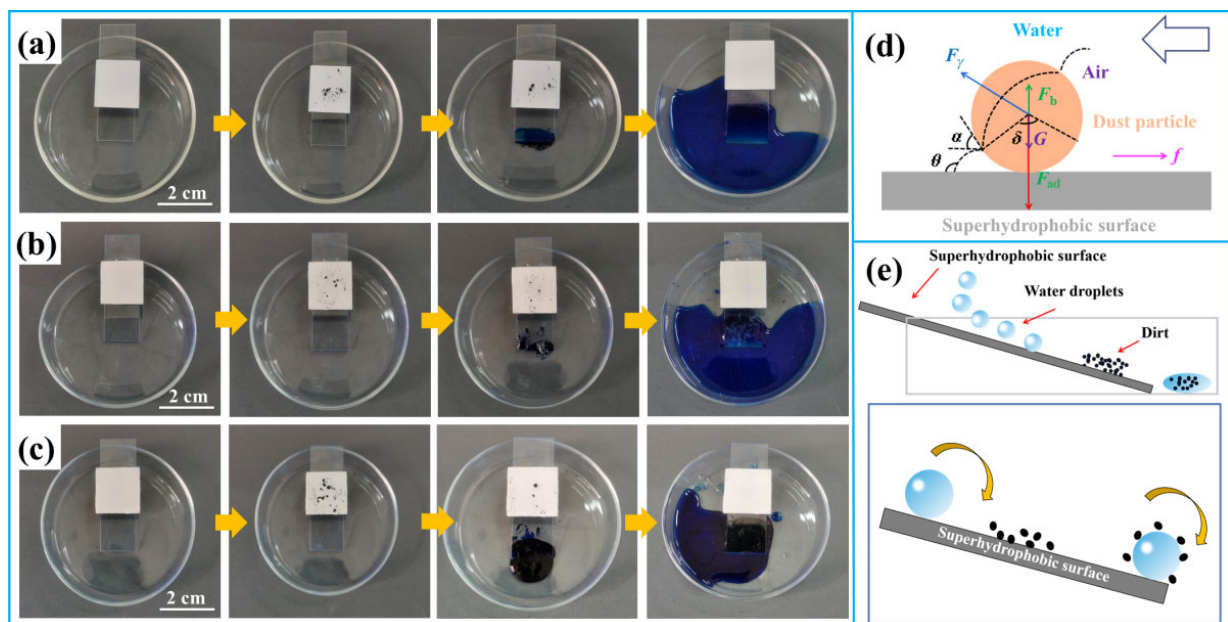

Fig. 12 Self-cleaning processes of (a) decoupling, (b) nano, and (c) coupling coatings. (d) Force analysis of a particle leaving off a superhydrophobic surface. Reproduced with permission from Ref. [59], ©American Chemical Society 2017. (e) Self-cleaning mechanism of the superhydrophobic surface.
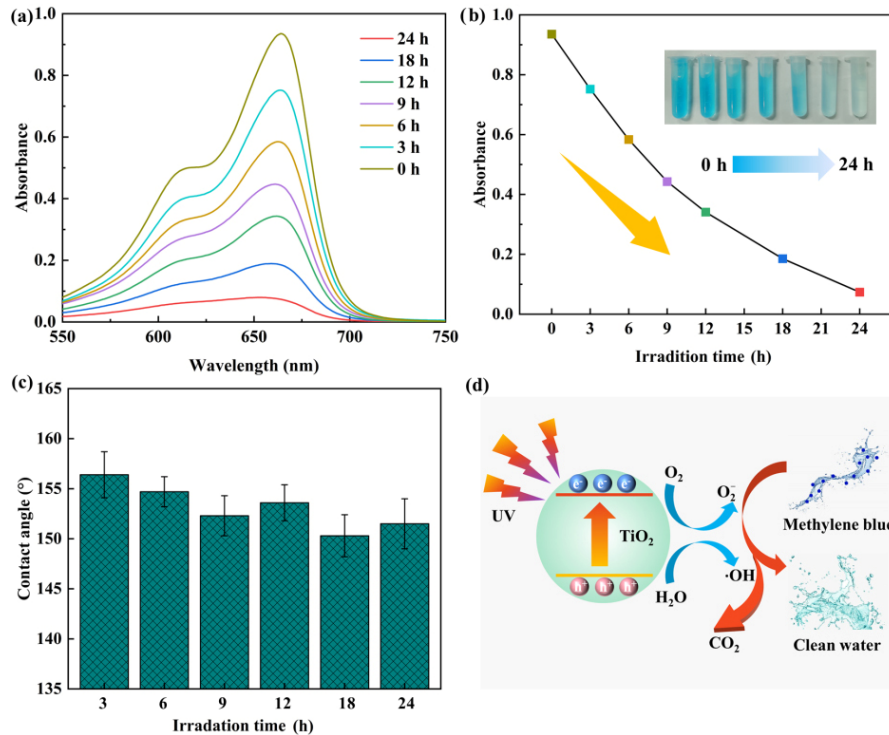
Fig. 13 (a) Absorption spectra of MB solution exposing UV at different irradiation times. (b) Absorption and colors of MB solution as a function of time. (c) CAs of the decoupling coating after immersion in MB solution for different times. (d) Mechanism of photocatalytic degradation for MB solution by the decoupling coating.

TiO_2 particle surface after irradiated by high-energy UV light. They react with O_2 and H_2O of the external environment to transform into a mass of reactive radicals. These reactive free radicals decompose organics in seawater into small molecules such as CO_2, H_2O, etc., achieving photocatalytic degradation. Thus, the decoupling superhydrophobic coating shows outstanding photocatalytic degradation due to the existence of TiO_2 nano particles, which improves its self-cleaning property.

3.5 Antifouling property of decoupling superhydrophobic coating

Biofouling imposes negative impacts on Al alloy substrate and is related to surface wettability [62, 63]. To characterize the anti-biofouling property of the decoupling superhydrophobic coating, the decoupling and coupling samples were both immersed into seawater. Figure 14(b) shows the SEM image of the decoupling coating after immersion in seawater for 7 d. There are no microbial impurities on the surface of the decoupling coating. Moreover, the superhydrophobicity of the decoupling coating maintains, with the CA still

above 150° and the RA below 5° (Fig. S12 in the ESM). It indicates that the decoupling superhydrophobic coating effectively inhibits biofouling. In addition, the coupling coating also shows noticeable antifouling property (Fig. 14(d)). The proposed mechanism for
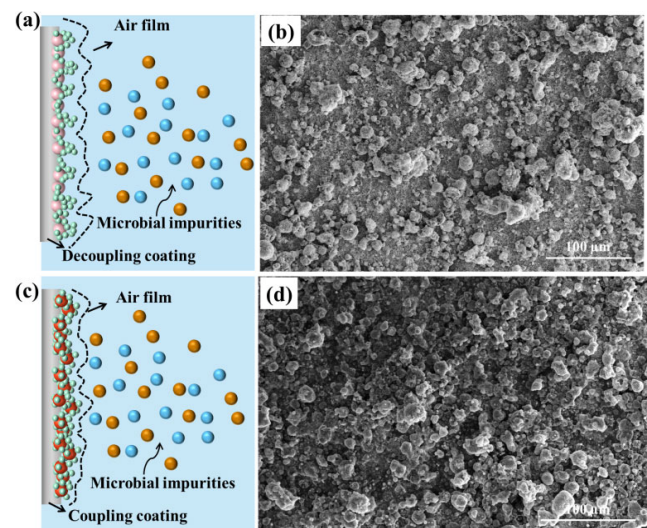

Fig. 14 Antifouling mechanism of (a) decoupling coating and (c) coupling coating; SEM images of (b) decoupling coating and (d) coupling coating after immersion into seawater for 7 d.

antifouling is shown in Figs. 14(a) and 14(c). The superhydrophobic decoupling and coupling coatings both exhibit micro-nano composite structures, which contributes to a large amount of air trapped into gaps of micro-nano structures. The trapped air reduces the surface-liquid area and prevents the penetration of microbial impurities into the gaps of micro-nano structures [62, 63], endowing the coating with its outstanding antifouling property. Thus, the decoupling coating and the coupling coating both show promising antifouling property.

4   Conclusions

In summary, to improve robustness of the superhydrophobic coating and expand its application, we demonstrated a simple method to fabricate a robust decoupling superhydrophobic coating on Al alloy substrate. The EP coating was first dripped on Al alloy substrate as the adhesive layer. After reaching the semi-cured state, unmodified micro SiO_2 particles were sprayed on the adhesive layer, which promised the robustness. Then, the modified nano TiO_2 particles were quickly sprayed on the surface, which provided the hydrophobicity. We confirmed the water repellency, adhesion strength, wear resistance, drag reduction, self-cleaning, and antifouling properties of the prepared decoupling superhydrophobic coating by comparing with other two superhydrophobic coatings—nano and coupling superhydrophobic coatings. The decoupling superhydrophobic coating exhibits high repellency for impacting water droplets. Notably, this decoupling coating shows outstanding adhesion strength on substrate after tape peeling and cross-cut tests, and displays promising wear resistant after sandpaper abrasion and wear test, with the friction coefficient of only ~0.2. Moreover, the robust decoupling superhydrophobic coating is applied to underwater buoyancy enhancement and fluid resistance reduction (drag reduction rate: ~30.09%). This decoupling superhydrophobic coating also shows promising self-cleaning and antifouling properties. Moreover, the decoupling coating is also exploited for degrading organics to achieve seawater purification due to the photocatalytic property of TiO_2 nano particles. We believe that this decoupling superhydrophobic coating is expected to provide new solutions for drag reduction, self-cleaning, and antifouling properties of metal materials in marine fields, and the simple and eco-friendly method develops potential practical application.

Declaration of competing interest

The authors have no competing interests to declare that are relevant to the content of this article.

Electronic Supplementary Material Supplementary material is available in the online version of this article at https://doi.org/10.1007/s40544-022-0652-3.

References

[1] Chen S W, Zhu M H, Zhang Y H, Dong S, Wang X J. Magnetic-responsive superhydrophobic surface of magnetorheological elastomers mimicking from lotus leaves to rose petals. *Langmuir* **37**(7): 2312–2321 (2021)

[2] Wang X, Ding H, Sun S J, Zhang H, Zhou R, Li Y Z, Liang Y, Wang J. Preparation of a temperature-sensitive superhydrophobic self-cleaning SiO$_2$–TiO$_2$@PDMS coating with photocatalytic activity. *Surf Coat Technol* **408**: 126853 (2021)

[3] Yin X L, Yu S R, Wang K, Cheng R C, Lv Z X. Fluorine-free preparation of self-healing and anti-fouling superhydrophobic Ni$_3$S$_2$ coating on 304 stainless steel. *Chem Eng J* **394**: 124925 (2020)

[4] Wang Y H, Zhang Z B, Xu J K, Yu H D. One-step method using laser for large-scale preparation of bionic superhydrophobic & drag-reducing fish-scale surface. *Surf Coat Technol* **409**: 126801 (2021)

[5] Zhang L S, Zhou A G, Sun B R, Chen K S, Yu H Z. Functional and versatile superhydrophobic coatings via stoichiometric silanization. *Nat Commun* **12**: 982 (2021)

[6] Zhang J X, Zhang L G, Gong X. Large-scale spraying fabrication of robust fluorine-free superhydrophobic coatings based on dual-sized silica particles for effective antipollution and strong buoyancy. *Langmuir* **37**(19): 6042–6051 (2021)

[7] Li H, Yu S R, Hu J H, Yin X L. Modifier-free fabrication of durable superhydrophobic electrodeposited Cu–Zn coating on steel substrate with self-cleaning, anti-corrosion and anti-scaling properties. *Appl Surf Sci* **481**: 872–882 (2019)

[8] Zhang H, Hou C P, Song L X, Ma Y, Ali Z, Gu J W, Zhang B L, Zhang H P, Zhang Q Y. A stable 3D sol–gel network with dangling fluoroalkyl chains and rapid self-healing ability as a long-lived superhydrophobic fabric coating. *Chem Eng J* **334**: 598–610 (2018)

[9] Wu B R, Lyu J J, Peng C Y, Jiang D Z, Yang J, Yang J S, Xing S L, Sheng L P. Inverse infusion processed hierarchical structure towards superhydrophobic coatings with ultrahigh mechanical robustness. *Chem Eng J* **387**: 124066 (2020)

[10] Ma D D, Lin H C, Hei H J, Ma Y, Gao J, Zhang M, Yu S W, Xue Y P, Tang B. Fabrication of porous micro/nano structured Cr coating with superhydrophobic and ultrahigh adhesion properties by plasma reverse sputtering process. *Vacuum* **201**: 111049 (2022)

[11] Wang D H, Sun Q Q, Hokkanen M J, Zhang C L, Lin F Y, Liu Q, Zhu S P, Zhou T F, Chang Q, He B, et al. Design of robust superhydrophobic surfaces. *Nature* **582**(7810): 55–59 (2020)

[12] Li D W, Wang H Y, Liu Y, Wei D S, Zhao Z X. Large-scale fabrication of durable and robust super-hydrophobic spray coatings with excellent repairable and anti-corrosion performance. *Chem Eng J* **367**: 169–179 (2019)

[13] Wang Z C, Liu X J, Ji J W, Tao T T, Zhang T, Xu J M, Jiao Y L, Liu K. Underwater drag reduction and buoyancy enhancement on biomimetic antiabrasive superhydrophobic coatings. *ACS Appl Mater Interfaces* **13**(40): 48270–48280 (2021)

[14] Li H, Xin L, Zhang K, Yin X L, Yu S R. Fluorine-free fabrication of robust self-cleaning and anti-corrosion superhydrophobic coating with photocatalytic function for enhanced anti-biofouling property. *Surf Coat Technol* **438**: 128406 (2022)

[15] Ye H, Zhu L Q, Li W P, Liu H C, Chen H N. Constructing fluorine-free and cost-effective superhydrophobic surface with normal-alcohol-modified hydrophobic SiO$_2$ nanoparticles. *ACS Appl Mater Interfaces* **9**(1): 858–867 (2017)

[16] Rong W T, Zhang H F, Mao Z G, Chen L, Liu X W. Improved stable drag reduction of controllable laser-patterned superwetting surfaces containing bioinspired micro/nanostructured arrays. *ACS Omega* **7**(2): 2049–2063 (2022)

[17] Bai Y X, Zhang H P, Shao Y Y, Zhang H, Zhu J. Recent progresses of superhydrophobic coatings in different application fields: An overview. *Coatings* **11**(2): 116 (2021)

[18] Zahrim A Y, Tizaoui C, Hilal N. Coagulation with polymers for nanofiltration pre-treatment of highly concentrated dyes: A review. *Desalination* **266**(1–3): 1–16 (2011)

[19] Ghosh S, Kouamé N A, Ramos L, Remita S, Dazzi A, Deniset-Besseau A, Beaunier P, Goubard F, Aubert P H, Remita H. Conducting polymer nanostructures for photocatalysis under visible light. *Nat Mater* **14**(5): 505–511 (2015)

[20] Wakerley D, Lamaison S, Ozanam F, Menguy N, Mercier D, Marcus P, Fontecave M, Mougel V. Bio-inspired hydrophobicity promotes CO$_2$ reduction on a Cu surface. *Nat Mater* **18**(11): 1222–1227 (2019)

[21] Li F R, Kong W T, Zhao X Z, Pan Y L. Multifunctional TiO$_2$-based superoleophobic/superhydrophilic coating for oil–water separation and oil purification. *ACS Appl Mater Interfaces* **12**(15): 18074–18083 (2020)

[22] Islam M T, Dominguez A, Turley R S, Kim H, Sultana K A, Shuvo M, Alvarado-Tenorio B, Montes M O, Lin Y R, Gardea-Torresdey J, et al. Development of photocatalytic paint based on TiO$_2$ and photopolymer resin for the degradation of organic pollutants in water. *Sci Total Environ* **704**(20): 135406 (2019)

[23] Pan R, Cai M Y, Liu W J, Luo X, Chen C H, Zhang H J, Zhong M L. Extremely high Cassie–Baxter state stability of superhydrophobic surfaces via precisely tunable dual-scale and triple-scale micro-nano structures. *J Mater Chem A* **7**(30): 18050–18062 (2019)

[24] Li H, Peng Y J, Yu S R, Yin X L. Both slender pillars and hierarchical structures achieving superhydrophobicity and the comparison of their properties. *Appl Surf Sci* **505**: 144524 (2020)

[25] Mokoba T, Lu J F, Zhang T C, Ouyang L K, Yuan S J. Superhydrophobic ODT-TiO$_2$ NW-PDA nanocomposite-coated polyurethane sponge for spilled oil recovery and oil/water separation. *Colloids Surf A Physicochem Eng Aspects* **630**(5): 127541(2021)

[26] Qing Y Q, Yang C N, Yu N N, Shang Y, Sun Y Z, Wang L S, Liu C S. Superhydrophobic TiO$_2$/polyvinylidene fluoride composite surface with reversible wettability switching and corrosion resistance. *Chem Eng J* **290**(15): 37–44 (2016)

[27] Lu J F, Liu X, Zhang T C, He H Q, Yuan S J. Magnetic superhydrophobic polyurethane sponge modified with bioinspired stearic acid@Fe$_3$O$_4$@PDA nanocomposites for oil/water separation. *Colloids Surf A Physicochem Eng Aspects* **624**(5): 126794 (2021)

[28] Li K K, Xie Y X, Lei J, Zhang S H, Liu Z, Lu L S. An inspiration from purple orchid leaves: Surface characteristics and wettability of nanoscale organometallic coatings electrodeposited on laser-patterned microstructures. *Surf Coat Technol* **427**: 127817 (2021)

[29] Li H, Zhang K. Dynamic behavior of water droplets impacting on the superhydrophobic surface: Both experimental study and molecular dynamics simulation study. *Appl Surf Sci* **498**: 143793 (2019)

[30] Liu Y H, Moevius L, Xu X P, Qian T Z, Yeomans J M, Wang Z K. Pancake bouncing on superhydrophobic surfaces. *Nat Phys* **10**(7): 515–519 (2014)

[31] Li H, Yan T Y, Fichthorn K A. Influence of gravity on the sliding angle of water drops on nanopillared superhydrophobic surfaces. *Langmuir* **36**(33): 9916–9925 (2020)

[32] Qu M N, Ma X R, He J M, Feng J, Liu S S, Yao Y L, Hou L G, Liu X R. Facile selective and diverse fabrication of superhydrophobic, superoleophobic-superhydrophilic and superamphiphobic materials from Kaolin. *ACS Appl Mater Interfaces* **9**(1): 1011–1020 (2017)

[33] Zong L J, Wu Y P, Li X G, Jiang B. The preparation of superhydrophobic photocatalytic fluorosilicone/SiO$_2$–TiO$_2$ coating and its self-cleaning performance. *J Coat Technol Res* **18**(5): 1245–1259 (2021)

[34] Yu M N, Liu M M, Zhang D D, Fu S H. Lubricant-grafted omniphobic surfaces with anti-biofouling and drag-reduction performances constructed by reactive organic–inorganic hybrid microspheres. *Chem Eng J* **422**: 130113 (2021)

[35] Xue F X, Shi X T, Bai E X, Li J E, Li Y W, Zhu S Y, Liu Y H, Feng L B. Enhanced durability and versatile superhydrophobic coatings via facile one-step spraying technique. *Colloids Surf A Physicochem Eng Asp* **640**: 128411 (2022)

[36] Huang S, Fang Z P, Chen D, Yu Z K, Sun Z G, Zhang Y H. Fabrication of mechanochemically robust superhydrophobic coating based on MPVDF/epoxy resins composites. *Prog Org Coat* **163**: 106651 (2022)

[37] Wang Z H, Yuan L, Liang G Z, Gu A J. Mechanically durable and self-healing super-hydrophobic coating with hierarchically structured KH570 modified SiO$_2$-decorated aligned carbon nanotube bundles. *Chem Eng J* **408**: 127263 (2021)

[38] Lin D, Zhang X G, Yuan S C, Li Y, Xu F, Wang X, Li C, Wang H Y. Robust waterborne superhydrophobic coatings with reinforced composite interfaces. *ACS Appl Mater Interfaces* **12**(42): 48216–48224 (2020)

[39] Li C L, Sun Y C, Cheng M, Sun S Q, Hu S Q. Fabrication and characterization of a TiO$_2$/polysiloxane resin composite coating with full-thickness super-hydrophobicity. *Chem Eng J* **333**: 361–369 (2018)

[40] Wu C Q, Liu Q, Chen R R, Liu J Y, Zhang H S, Li R M, Takahashi K, Liu P L, Wang J. Fabrication of ZIF-8@SiO$_2$ micro/nano hierarchical superhydrophobic surface on AZ31 magnesium alloy with impressive corrosion resistance and abrasion resistance. *ACS Appl Mater Interfaces* **9**(12): 11106–11115 (2017)

[41] Sun J F, Wang W Q, Liu Z, Li B, Xing K F, Yang Z. Study on selective laser melting 316L stainless steel parts with superhydrophobic surface. *Appl Surf Sci* **533**: 1447445 (2022)

[42] Liu T L, Kim C J. Turning a surface superrepellent even to completely wetting liquids. *Science* **346**(6213): 1096–1100 (2014)

[43] Zhang W B, Xiang T H, Liu F, Zhang M, Gan W T, Zhai X L, Di X, Wang Y Z, Liu G X, Wang C Y. Facile design and fabrication of superwetting surfaces with excellent wear-resistance. *ACS Appl Mater Interfaces* **9**(18): 15776–15784 (2017)

[44] Kondrashov V, Rühe J. Microcones and nanograss: Toward mechanically robust superhydrophobic surfaces. *Langmuir* **30**(15): 4342–4350 (2014)

[45] Hwang G B, Patir A, Page K, Lu Y, Allan E, Parkin I P. Buoyancy increase and drag-reduction through a simple superhydrophobic coating. *Nanoscale* **9**(22): 7588–7594 (2017)

[46] Yin K, Dong X R, Zhang F, Wang C, Duan J A. Superamphiphobic miniature boat fabricated by laser micromachining. *Appl Phys Lett* **110**(12): 121909 (2017)

[47] Gao X F, Jiang L. Water-repellent legs of water striders. *Nature* **432**(7013): 36 (2004)

[48] Peng C Y, Chen Z Y, Tiwari M K. All-organic superhydrophobic coatings with mechanochemical robustness and liquid impalement resistance. *Nat Mater* **17**(4): 355–360 (2018)

[49] Martouzet G, Lee C, Pirat C, Ybert C, Biance A L. Drag reduction on drop during impact on multiscale superhydrophobic surfaces. *J Fluid Mech* **892**: R2 (2020)

[50] Liu Y B, Gu H M, Jia Y, Liu J, Zhang H, Wang R M, Zhang B L, Zhang H P, Zhang Q Y. Design and preparation of biomimetic polydimethylsiloxane (PDMS) films with superhydrophobic, self-healing and drag reduction properties via replication of shark skin and SI-ATRP. *Chem Eng J* **356**: 318–328 (2019)

[51] Dong H Y, Cheng M J, Zhang Y J, Wei H, Shi F. Extraordinary drag-reducing effect of a superhydrophobic coating on a macroscopic model ship at high speed. *J Mater Chem A* **1**(19): 5886–5891 (2013)

[52] Rad S V, Moosavi A, Nouri-Boroujerdi A, Najafkhani H, Najafpour S. Drag reduction in internal turbulent flow by fabricating superhydrophobic Al_2O_3/waterborne polyurethane coatings. *Surf Coat Technol* **421**: 127406 (2021)

[53] Tuo Y J, Zhang H F, Rong W T, Jiang S Y, Chen W P, Liu X W. Drag reduction of anisotropic superhydrophobic surfaces prepared by laser etching. *Langmuir* **35**(34): 11016–11022 (2019)

[54] Liu Y B, Liu J, Tian Y, Zhang H, Wang R M, Zhang B L, Zhang H P, Zhang Q Y. Robust organic–inorganic composite films with multifunctional properties of superhydrophobicity, self-healing, and drag reduction. *Ind Eng Chem Res* **58**(11): 4468–4478 (2019)

[55] Rong W T, Zhang H F, Mao Z G, Chen L, Liu X W. Stable drag reduction of anisotropic superhydrophobic/hydrophilic surfaces containing bioinspired micro/nanostructured arrays by laser ablation. *Colloids Surf A Physicochem Eng Aspects* **622**: 126712 (2021)

[56] Ahmad Kamal S A, Ritikos R, Abdul Rahman S. Enhancement of self-cleaning properties and durability of super-hydrophobic carbon nitride nanostructures by post-annealing treatment. *Surf Coat Technol* **409**: 126912 (2021)

[57] Anjum A S, Sun K C, Ali M, Riaz R, Jeong S H. Fabrication of coral-reef structured nano silica for self-cleaning and super-hydrophobic textile applications. *Chem Eng J* **401**: 125859 (2020)

[58] Qu Z Y, Wang F Z, Liu P, Yu Q L, Brouwers H J H. Super-hydrophobic magnesium oxychloride cement (MOC): From structural control to self-cleaning property evaluation. *Mater Struct* **53**: 30 (2020)

[59] Yu M, Chen S, Zhang B, Qiu D L, Cui S X. Why a lotus-like superhydrophobic surface is self-cleaning? An explanation from surface force measurements and analysis. *Langmuir* **30**(45): 13615–13621 (2014)

[60] Liu N, Zhang Q D, Qu R X, Zhang W F, Li H F, Wei Y, Feng L. Nanocomposite deposited membrane for oil-in-water emulsion separation with *in situ* removal of anionic dyes and surfactants. *Langmuir* **33**(30): 7380–7388 (2017)

[61] Gao C R, Sun Z X, Li K, Chen Y N, Cao Y Z, Zhang S Y, Feng L. Integrated oil separation and water purification by a double-layer TiO_2-based mesh. *Energy Environ Sci* **6**(4): 1147–1151 (2013)

[62] Tian J Y, Zhao Y Y, Wu L L, Deng X H, Zhao Z J, Zhang C C. Preparation of refreshable membrane by partially sacrificial hydrophilic coating. *J Mater Sci* **56**(17): 10676–10690 (2021)

[63] Yin Z Z, Yuan F, Xue M S, Xue Y H, Xie Y, Ou J F, Luo Y D, Hong Z, Xie C. A multifunctional and environmentally safe superhydrophobic membrane with superior oil/water separation, photocatalytic degradation and anti-biofouling performance. *J Colloid Interf Sci* **611**: 93–104 (2022)

Lei XIN. She is currently a master candidate at Shandong University of Science and Technology, China, under the supervision of associate Professor Hao LI. Her current scientific interests are focused on the superhydrophobic surface on metal materials.

Hao LI. She received her Ph.D. degree from China University of Petroleum (East China) in 2017. She visited the Pennsylvania State University, University Park, USA, from 2016 to 2017. Now she is an associate professor of Shandong University of Science and Technology, China. Her current scientific interests are focused on the surfaces and interfaces of the bionic wettability materials.

Zhongwei WANG. He received his Ph.D. degree from Beijing Institute of Technology, China, in 2004. Now he is a professor of Shandong University of Science and Technology, China. His current scientific interests are focused on the synthesis and application of organic polymer materials.

Sirong YU. He received his Ph.D. degree from Harbin Institute of Technology, China, in 1996. From February 2004 to January 2005, he was invited as a visiting scholar at Center for Advanced Materials Technology in School of Aerospace, Mechanical and Mechatronic Engineering in The University of Sydney, Austrilia. Now he is a professor and doctoral supervisor in School of Materials Science and Engineering, China University of Petroleum (East China). His current research interests are the casting alloy materials, metal matrix composites, friction and wear of materials, and surface engineering.